Biophysical Study of Thermal Denaturation of Apo-Calmodulin: Dynamics of Native and Unfolded States

Gabriel Gibrat,* France Liliane Assairi,† Yves Blouquit,† Constantin T. Craescu,† and Marie-Claire Bellissent-Funel*

*Laboratoire Léon Brillouin, Commissariat à l'Energie Atomique/Centre National de la Recherche Scientifique, Saclay, France; and †INSERM U759/Institut Curie-Recherche, Orsay, France

ABSTRACT Apo-calmodulin, a small, mainly α, soluble protein is a calcium-dependent protein activator. This article presents a study of internal dynamics of native and thermal unfolded apo-calmodulin, using quasi-elastic neutron scattering. This technique can probe protein internal dynamics in the picosecond timescale and in the nanometer length-scale. It appears that a dynamical transition is associated with thermal denaturation of apo-calmodulin. This dynamical transition goes together with a decrease of the confinement of hydrogen atoms, a decrease of immobile protons proportion and an increase of dynamical heterogeneity. The comparison of native and unfolded states dynamics suggests that the dynamics of protein atoms is more influenced by their distance to the backbone than by their solvent exposure.

INTRODUCTION

The protein folding problem

The importance of protein folding or the ability of a protein to fold reliably into a predetermined conformation despite a near infinite number of possibilities is, despite much research, still poorly understood. It has long been known that the structure of a protein is determined purely by the amino-acid sequence, and the structure of the protein determines the function. By extension, the function of a protein depends entirely on the ability of the protein to fold rapidly and reliably to its native structure. The protein folding problem has not yet been solved. A complete understanding of protein folding requires the physical characterization of both native and denatured states and evaluation of the thermodynamic states of the system. In the cell, proteins are synthesized in a linear way. However, for most of them, their biological function is given by their structure. Understanding the sequence-structure relationship is thus essential for biology. This is the reason for which protein folding and unfolding have been studied from many years (1–7). Most studies are concerned with the structural and thermodynamic aspects of folding and unfolding. However, it has been shown that protein internal dynamics has an influence on protein activity (8–10) such that recently, some studies focus on internal dynamics of native and denatured or unfolded states (11,12). In this frame, this article presents a study of dynamics of native and thermal unfolded apo-calmodulin.

Calmodulin: a good model system

Calmodulin is a small (17 kDa) soluble calci-protein that can fix four calcium ions. Calcium fixation induces structural changes (13) and exposure of hydrophobic patches (14), allowing calmodulin to fix to target peptides and to activate them. That is why calmodulin is called the ''ubiquitous intracellular eukaryotic calcium signal receptor and enzyme activator'' (15). The word ''ubiquitous'' means that calmodulin intervenes in a lot of various cellular mechanisms as the synthesis and the release of neurotransmitters, the regulation of intracellular calcium concentration, the muscle contraction, the cellular division, the cellular motility, etc. (16,17). Calmodulin thus exists in two distinct forms: the calcium free form, also called apo form, and the calcium saturated one, also called holo form. Since the holo form has been found to be exceptionally stable, holo-calmodulin thermal denaturation study is nearly impossible. In fact, holo-calmodulin can be exposed to temperatures higher than 90°C without any detectable change in its secondary or tertiary structure (18). On the contrary, thermal denaturation of apo-calmodulin has already been studied from a thermodynamic point of view (15,19,20). Results about conformation of native and denatured states are presented in an article to be published (G. Gibrat, Y. Blouquit, C. T. Craescu, and M.-C. Bellissent-Funel). As thermodynamic and structural aspects of thermal denaturation of apo-calmodulin have been studied, the next step was to study dynamics of thermal unfolded states. Apo-calmodulin is fully unfolded at ~80°C. The dynamics of unfolded states will be compared to that of the native state.

In that same unpublished article, it has been shown that, due to its high charge, calmodulin has a good colloidal stability in physiological-like pH (pH = 7.6) and ionic strength conditions (50 mM Tris and 80 mM KCl). It has also been emphasized that this colloidal stability was essential for studying thermal denaturation. This aspect is much more crucial when studying dynamics of native and especially thermal denatured states using quasi-elastic neutron scattering (QENS). Indeed,

Submitted August 18, 2007, and accepted for publication October 10, 2007.

Address reprint requests to Gabriel Gibrat, Tel.: 33-01-69-08-4042; E-mail: gabriel.gibrat@cea.fr.

Editor: Jill Trewhella.

0006-3495/08/12/5247/10 $2.00

doi: 10.1529/biophysj.107.120147

this technique requires high protein concentration of ~80 g/L. At such high concentrations, aggregation of thermal unfolded proteins can easily occur, since thermal unfolding exposes hydrophobic parts at the protein surface and increases the volume occupied by the protein. It results in an increase of the attractive part of the interprotein potential and a decrease of the mean distance between proteins. The high interprotein electrostatic repulsion in the case of apo-calmodulin solutions with physiological-like pH and ionic strength avoids this aggregation as shown later. This makes apo-calmodulin a good system for studying dynamics of thermal denatured states using QENS.

METHODS

Sample realization

Human CaM cDNA was amplified by PCR, and inserted into the vector pET24a (Novagen, Madison, WI) (between the *Nde*I and *Xho*I restriction sites). The resulting plasmid was introduced into the strain Bl21(DE3)/pDIA17 to overproduce human CaM. The recombinant strain was grown in 2× yeast extract tryptone medium supplemented with kanamycin (70 μg/mL) and chloramphenicol (30 μg/mL) to an absorbance of 1.5 at 600 nm, and then overproduction was induced by isopropyl β-D-thiogalactopyranoside (1 mM final concentration) for 3 h at 37°C. The protein purification was performed using three chromatographic steps including DEAE-TSK, phenyl-TSK, and G25 columns (22). After lyophilization, the appropriate amount of protein is solubilized in the chosen buffer to obtain the desired concentration. To eliminate all the calcium present in the lyophilized powder, as well as all the labile protein protons, the solution is dialyzed at least 4 h (per bath) in three baths (with a volume 100 times larger than that of the solution) of D_2O buffer with decreasing EDTA concentrations: 10 mM, 2 mM, and 500 μM. The longer hydrogen exchange time reported by Tjandra et al. (23) is ~3 h, and most of the exchange times reported by the same authors are shorter than 1 h. One can assert that after 12 h the amount of residual labile protons in the protein is <1%, and can be neglected. Then the concentration is determined by measuring the optical density at 280 nm and the solution is diluted again with the last dialysis bath to adjust the concentration. The last dialysis bath is kept to be measured as a blank for the standard corrections required by the different experiments.

Quasi-elastic neutron scattering (QENS) experiments

Quasi-elastic neutron scattering experiments were carried out on MIBEMOL spectrometer of the reactor Orphée (Laboratoire Léon Brillouin, CEA-CNRS, Saclay, France), at $\lambda = 5$ Å, with a resolution of 180 μeV (full width at half-maximum) in a Q-range lying between 0.5 Å^{-1} and 2.4 Å^{-1}. Apo-calmodulin dynamics has been investigated by measuring QENS spectra of a 5.7 mM (86 g/L) apo-calmodulin solution in 50 mM D_2O Tris buffer at pH = 7.6 (or pD = 7.6) with 80 mM of KCl and 500 μM of EDTA. Measurements on apo-calmodulin and on the corresponding buffer have been carried out at 15°C, 50°C, and 70°C. Small angle neutron scattering (SANS) spectra of the solution have been recorded at room temperature after the experiment to check the presence of eventual aggregates. Since the protein concentration is really high, the SANS spectra exhibit a huge structure factor but no evidence of aggregates. Moreover, the solution was still transparent. All experimental QENS spectra were corrected according to the usual way (11,24): detector efficiency correction using vanadium, absorption correction and subtraction of buffer and empty cell. The treatment and analysis have been performed using the LAMP (25) and Qens_fit (26) programs.

Quasi-elastic neutron scattering (QENS) theory

A description of quasi-elastic neutron scattering technique can be found in Bée (27). For a review on its application to the study of protein dynamics, see Smith (28). In this subsection, we will shortly recall some basic notions. In a neutron scattering experiment, a sample is irradiated by a monochromatic incident neutron beam, characterized by a wavevector $\vec{k}_i$ and an energy $E_i = \hbar\omega_i$, where $\hbar$ is the Planck constant. The neutrons are scattered by the sample and exchange thus momentum and energy with the sample. The energy transfer is $\hbar\omega = \hbar\omega_i - \hbar\omega_f$, where $E_f = \hbar\omega_f$ is the energy of the scattered neutrons. One defines the momentum transfer as $\vec{Q} = \vec{k}_f - \vec{k}_i$, with $\vec{k}_f$ the wavevector of scattered neutrons. In case of elastic scattering (i.e., $\hbar\omega = 0$), one gets $|\vec{Q}| = Q_o = ((4\pi)/\lambda_i)\sin(\theta/2)$, with θ the scattering angle and λ_i the wavelength of the incident neutrons.

Coherent and incoherent scattering

Neutrons interact with the spin of the atom nucleus by strong interaction. Since the spin state of the atoms nuclei can change after interaction with neutrons, there are two kinds of scattering: the coherent scattering and the incoherent scattering. The coherent scattering of neutrons is comparable to light scattering or x-ray scattering and gives rise to interferences between waves scattered by different atoms. Incoherent scattering does not give rise to interferences, and depends only on the correlations between the position of the i^{th} atom at time t and the position of the same atom at time t'. Coherent and incoherent neutron scattering are characterized respectively by the coherent and incoherent scattering length, b_{coh} and b_{inc}. An interesting point for the study of dynamics of soft matter in general, and proteins in particular, using neutron scattering is the balance of coherent and incoherent scattering length of atoms constituting organic molecules. Indeed, as shown in Table 1, hydrogen, that is, the main component of organic molecules, has a huge incoherent scattering cross section σ_H^{inc} when compared to that of other atoms. For a 10 g/L calmodulin solution, the incoherent intensity scattered by the protein is ~3.10^{-3} cm^{-1}. As shown in our unpublished results (G. Gibrat, Y. Blouquit, C. T. Craescu, and M.-C. Bellissent-Funel), relative to structural aspects of thermal denaturation of apo calmodulin, the coherent intensity scattered by the native protein at $Q = 0.2$ Å^{-1} is equal to $1.5.10^{-2}$ cm^{-1} and decreases as Q^{-4} for Q values >0.2 Å^{-1}, leading to a value of the coherent intensity as low as 3.10^{-5} cm^{-1} at $Q = 1$ Å^{-1}. In the case of the thermal denatured protein, the coherent intensity at $Q = 0.2$ Å^{-1} is equal to 6.10^{-3} cm^{-1} and decreases as $Q^{-2.3}$, leading to a value of $1.5.10^{-4}$ cm^{-1} at $Q =$ 1 Å^{-1}. Thus, in the Q-range of the QENS experiment, one can consider that the scattered intensity is purely incoherent. The notation is $I_{inc}(\vec{Q},\omega)$. In fact, $I_{inc}(\vec{Q},\omega)$ is largely dominated by the contribution of hydrogen atoms of the protein that represents 99% of the total incoherent scattering cross section of the protein.

Van Hove formalism

In a QENS experiment, the scattered intensity $I(\vec{Q},\omega)$ is proportional to the differential scattering cross section, $d^2\sigma/d\Omega d\omega$. Since in our experiment the scattered intensity is purely incoherent, the measured quantity, $I_{inc}(\vec{Q},\omega)$ is proportional to the incoherent differential scattering cross section, $(d^2\sigma/d\Omega d\omega)_{inc}$,

$$I_{inc}(\vec{Q},\omega) \propto \left(\frac{d^2\sigma}{d\Omega d\omega}\right)_{inc} = N\frac{k_f}{2\pi k_i}\frac{\sigma_{inc}^H}{4\pi}S_{inc}(\vec{Q},\omega), \quad (1)$$

where

$$S_{inc}(\vec{Q},\omega) = \frac{1}{N}\int \sum_j e^{i\vec{Q}\vec{R}_j(0) - i\vec{Q}\vec{R}_j(t)} e^{-i\omega t} dt$$
$$= \frac{1}{N}\int\int G_s(\vec{r},t) e^{i(\vec{Q}.\vec{r}-\omega t)} d\vec{r}dt. \quad (2)$$

TABLE 1 Coherent and incoherent neutron scattering length, in Fermi (1 fm = 10^{-13} cm) of the main components of organic molecules

Element	C	N	O	S	H	D
b_{coh}(fm)	6.65	9.36	5.80	2.85	−3.74	6.67
b_{inc}(fm)	0	1.99	0	0	25.274	4.04
σ_{inc}(barn)	0	0.5	0	0	80.26	2.05
σ_{abs}(barn) (at 1.8 Å)	0	1.90	0	0	0.33	0

$S_{inc}(\vec{Q},\omega)$ is the incoherent dynamic structure factor, and is the space and time Fourier transform of the van Hove self-correlation function, $G_s(\vec{r},t)$; that is, simply the probability to find an atom at the position $\vec{r}$ and at the time t, knowing that the same atom was at the position $\vec{r}=\vec{0}$ at the time $t=0$. Thus, in a QENS experiment on proteins, one gets access to the individual dynamics of hydrogen atoms of protein. Since hydrogen atoms are uniformly distributed throughout the protein, they are a good probe of protein dynamics.

The incoherent dynamic structure factor

The measured incoherent scattering cross section is proportional to the incoherent dynamic structure factor, $S_{inc}(\vec{Q},\omega)$ (see Eq. 1). Since protein solutions are isotropic, $S_{inc}(\vec{Q},\omega)$ depends only on the norm of $\vec{Q}$, and will be written as $S_{inc}(Q,\omega)$. The analysis of QENS spectra requires a model for $S_{inc}(Q,\omega)$. In the quasi-elastic domain, the motions contributing to the incoherent dynamic structure factor are the diffusive ones (29). For proteins in solution, these motions are the global translational and rotational diffusion and the internal diffusive motions. It is generally assumed that these motions are uncoupled. The incoherent dynamic structure factor can be written as

$$S_{inc}(Q,\omega)=e^{-Q^2\langle u^2\rangle/3}\left[S_{inc}^{diff}(Q,\omega)\otimes S_{inc}^{rot}(Q,\omega)\otimes S_{inc}^{int}(Q,\omega)\right], \tag{3}$$

where $e^{-Q^2\langle u^2\rangle/3}$ is called the Debye-Waller factor, and $\langle u^2\rangle$ is the mean-square displacement. In the (Q,ω) space, a diffusive motion is associated with a normalized Lorentzian function, $\mathcal{L}(\Gamma,\omega)=(1/\pi)\cdot\Gamma/(\Gamma^2+\omega^2)$ (in the $(\vec{r},t)$ space; diffusive motions are associated with exponential relaxations $\propto e^{-\alpha(r)t}$) with a half-width at half-maximum Γ. There are exact expressions for the incoherent dynamic structure factor associated with global translation diffusion and rigid global rotation

$$S_{inc}^{diff}(Q,\omega)=\mathcal{L}_{diff}(DQ^2,\omega), \tag{4}$$

$$S_{inc}^{rot}(Q,\omega)=\mathcal{L}_{rot}(2D_r,\omega), \tag{5}$$

where D is the translational diffusion coefficient and D_r is the rotational diffusion coefficient. A model used to describe internal diffusive motions of proteins (11,30,31) is given by

$$S_{inc}^{int}(Q,\omega)=A(Q)\delta(\omega)+[1-A(Q)]\mathcal{L}_{int}(\Gamma_{int}(Q),\omega), \tag{6}$$

where $\mathcal{L}_{int}(\Gamma_{int}(Q),\omega)$ is the Lorentzian function of internal motions of protein and A is the elastic incoherent structure factor (EISF), a function that describes the geometry of the motions. Finally, from Eqs. 3–6, the model for protein incoherent dynamic structure factor in the quasi-elastic region can be expressed as

$$S_{inc}(Q,\omega)=e^{-Q^2\langle u^2\rangle/3}\mathcal{L}_{diff}(DQ^2,\omega)\otimes\mathcal{L}_{rot}(2D_r,\omega)\otimes\{A(Q)\delta(\omega)+[1-A(Q)]\mathcal{L}_{int}(\Gamma_{int}(Q),\omega)\}. \tag{7}$$

The model given by Eq. 7 can be simplified. Indeed, for apo-calmodulin, computer simulations give a rotational diffusion coefficient $D_r=0.04\ ns^{-1}$ (32). NMR experiments (33) give rotational correlation times τ_r of 6 ns, leading to a rotational diffusion coefficient $D_r=0.03\ ns^{-1}$ ($D_r=1/6\tau_r$). These two D_r values correspond to a full width $2*\Gamma_{rot}$ of the associated Lorentzian $\mathcal{L}_{rot}(2D_r,\omega)$ of 52 neV and 36 neV, respectively. Since the resolution of the experiment is 180 μeV, then $\mathcal{L}_{rot}(2D_r,\omega)$ can be approximated to a Dirac distribution $\delta(\omega)$, and the model becomes

$$S_{inc}(Q,\omega)=e^{-Q^2\langle u^2\rangle/3}\{A(Q)\mathcal{L}_{diff}(DQ^2,\omega)+[1-A(Q)]\mathcal{L}_{int}(\Gamma_{int}(Q)+DQ^2,\omega)\}. \tag{8}$$

By using appropriate models for $A(Q)$ and for the linewidth $\Gamma_{int}(Q)$ of internal motions, it was possible to fit the whole $S_{inc}(Q,\omega)$ spectra at once, using the model of Eq. 8. Since this model is reduced to two Lorentzian contributions, a step-by-step procedure, giving intermediate results, and thus more controlled, has been preferred. To increase statistics, data at different Q-values (or angles) were summed into 10 different groups. At each Q-value, grouped data have then been fitted with a sum of two nonnormalized Lorentzian functions, centered at $\omega=0$,

$$L_{diff}(\Gamma_{diff},\omega)=\frac{\mathcal{A}_{L_{diff}}(Q)}{\pi}\times\frac{\Gamma_{diff}}{\Gamma_{diff}+\omega^2}, \tag{9}$$

$$L_{int}(\Gamma_{diff}+\Gamma_{int},\omega)=\frac{\mathcal{A}_{L_{int}}(Q)}{\pi}\times\frac{\Gamma_{diff}+\Gamma_{int}}{\Gamma_{diff}+\Gamma_{int}+\omega^2}, \tag{10}$$

convoluted by the experimental resolution. The corrected experimental data, $I_{inc}(Q,\omega)$, are thus fitted using

$$I_{inc}(Q,\omega)=[L_{diff}(\Gamma_{diff}(Q),\omega)+L_{int}(\Gamma_{diff}(Q)+\Gamma_{int}(Q),\omega)]\otimes\mathcal{R}(\omega)+B(Q)\times\omega+C(Q) \tag{11}$$

with $B(Q)\times\omega+C(Q)$ as background. This fitting procedure gives Γ_{diff}, Γ_{int}, and the areas of the two Lorentzians $\mathcal{A}_{L_{diff}}$ and $\mathcal{A}_{L_{int}}$ for each Q-value. The identification of Eqs. 8 and 11 gives

$$L_{diff}(\Gamma_{diff},\omega)\propto e^{-Q^2\langle u^2\rangle/3}A(Q)\mathcal{L}_{diff}(DQ^2,\omega), \tag{12}$$

$$L_{int}(\Gamma_{diff}+\Gamma_{int},\omega)\propto e^{-Q^2\langle u^2\rangle/3}[1-A(Q)]\mathcal{L}_{int}(\Gamma_{int}(Q)+DQ^2,\omega). \tag{13}$$

Debye-Waller factor and mean-square displacements

By identifying Eqs. 8 and 11, one gets the Debye-Waller factor, $e^{-Q^2\langle u^2\rangle/3}$, that is extracted from the areas of the two Lorentzians, $\mathcal{A}_{L_{diff}}$ and $\mathcal{A}_{L_{int}}$:

$$DW(Q)=e^{-Q^2\langle u^2\rangle/3}\propto\mathcal{A}_{L_{diff}}(Q)+\mathcal{A}_{L_{int}}(Q). \tag{14}$$

However, it can also be obtained in a more direct way, before any fit of the QENS spectra. Indeed, if one integrates the Eq. 7, one gets

$$\int S_{inc}(Q,\omega)d\omega=e^{-Q^2\langle u^2\rangle/3}\int[A(Q)\mathcal{L}(DQ^2,\omega)+(1-A(Q))\mathcal{L}(\Gamma_{int}(Q)+DQ^2,\omega)]d\omega. \tag{15}$$

Since $\mathcal{L}(\Gamma,\omega)$ are normalized Lorentzians, $\int\mathcal{L}(\Gamma,\omega)d\omega=1$. This leads to

$$\int S_{inc}(Q,\omega)d\omega=e^{-Q^2\langle u^2\rangle/3}. \tag{16}$$

The Debye-Waller factor is thus directly proportional to the quasi-elastic intensity, $\int_{|\hbar\omega|\le 1\,meV}I_{inc}(Q,\omega)d\omega$, that can be easily computed, without any

fit and data grouping. This procedure allows us to get a model-independent determination of the mean-square displacement.

The elastic incoherent structure factor (EISF)

The EISF is a function describing the geometry of the internal motions. By identification of Eqs. 8 and 12, EISF can be obtained at each Q value, as

$$EISF(Q) = A(Q) = \frac{\mathcal{A}_{L_{diff}}(Q)}{\mathcal{A}_{L_{diff}}(Q) + \mathcal{A}_{L_{int}}(Q)}. \quad (17)$$

A biological system is characterized by a broad distribution of correlation times. The internal dynamics of the system is at the origin of the quasi-elastic signal that is well described by a single Lorentzian, i.e., a single correlation time as shown in Results and Discussion. Because of the finite resolution of the spectrometer, long correlation times contribute to a very narrow signal in energy centered about the elastic peak and are indistinguishable from it. It becomes therefore necessary to take into account a fraction p of protons seen as immobile at the resolution of the instrument (i.e., on a 5-ps timescale). The $(1-p)$ remaining protons fraction contribute also to the elastic peak through the pseudo-EISF, $A_0(Q)$, that can be seen as the form factor of the confinement volume of mobile protons. Finally, EISF can be expressed as

$$EISF(Q) = A(Q) = p + (1-p)A_0(Q). \quad (18)$$

An appropriate model for $A_0(Q)$ is given by the model of Volino and Dianoux (34), that has been successfully applied to describe the internal motions in proteins (11,24,30,31,35). This model considers atoms diffusing freely inside spheres of radius a with a diffusion coefficient D_{sph}, and leads to the expression for A_0,

$$A_0(Q) = \left(\frac{3j_1(Qa)}{Qa}\right)^2, \quad (19)$$

with j_1 a spherical Bessel function of the first kind: $j_1(x) = \sin x - x\cos x/x^2$. Using this pseudo-EISF, Eq. 18 becomes

$$EISF(Q) = A(Q) = p + (1-p)\left(\frac{3j_1(Qa)}{Qa}\right)^2. \quad (20)$$

Γ_{int} has the following properties:

$$\Gamma_{int}(Qa) = 4.33\frac{D_{sph}}{a^2} \quad \text{for} \quad Qa < \pi$$
$$\Gamma_{int}(Qa) = D_{sph}Q^2 \quad \text{for} \quad Qa \gg \pi. \quad (21)$$

Distribution of sphere radii

Proteins are complex systems, with long-chain residues as lysines or arginines, short-chain residues as alanine or glycine, and aromatic residues as phenylalanines or tyrosines. Roughly speaking, hydrophilic residues are exposed to solvent, while hydrophobic ones are buried in the protein interior. Thus, the dynamic behavior of protein protons is not expected to be homogeneous. As an example, Dellerue et al. (36) have shown for C-phycocyanin that the confinement radii of backbone protons and of side-chain protons were different. They have also shown that the confinement radii depend on the distance from the protein center of mass.

To describe the heterogeneity of protein protons dynamics, we have to consider an ensemble of spheres radii, and not a single sphere radius. Therefore, a model with a distribution of sphere radii, $P(a)$, will account more reliably for dynamics of proteins. The EISF (Eq. 20) becomes

$$A(Q) = p + (1-p)\int_0^\infty P(a)\left[\frac{3j_1(Qa)}{Qa}\right]^2 da \quad (22)$$

Instead of a Gaussian distribution, we have chosen a lognormal one, defined as

$$P(a) = \frac{1}{s\sqrt{2\pi}a} \times e^{-\frac{(\ln(a/c))^2}{2s^2}}, \quad (23)$$

where c is the median of the distribution, and s the variance in the natural logarithmic space. The mean of the distribution, μ, and the standard deviation, σ, can be obtained as

$$\mu = ce^{s^2}$$
$$\sigma = \mu\sqrt{e^{s^2} - 1}. \quad (24)$$

A lognormal distribution appears to be more appropriate than a Gaussian one to describe dynamics of protein protons at the resolution of our experiment. According to the energy resolution and the Q-range of our experiment, the motions investigated occur in the picosecond timescale and in the Å lengthscale. These motions corresponds to methyl rotation and side-chains librations (37). Carpentier et al. (38) has shown that the radius of the sphere of diffusion of a hydrogen atom along an aliphatic chain fixed at one end increases linearly with distance from the fixed end. The motions of hydrogens bound to the n^{th} carbon (starting from the fixed end) of the aliphatic chain are not independent of the motions of the hydrogens bound to the i^{th} carbon, $i < n$. In fact, the motions of the protons bound to the n^{th} carbon are the product of the motions of all the carbon atoms between the fixed end and the n^{th} carbon. A lognormal distribution results if the variable is the product of a large number of independent, identically distributed variables, while a Gaussian distribution results if the variable is the sum of a large number of independent, identically distributed variables. Thus a Gaussian distribution appears inadequate to account for side-chain proton motions, while the choice of a lognormal distribution appears more reasonable. Moreover, in the case of a lognormal distribution, $P(a=0) = 0$. Since an atom diffusing inside a sphere of null radius is an immobile atom, $P(a = 0)$ accounts for a proportion of immobile protons. But there is already a parameter in the EISF to account for the proportion of immobile protons: p. In other terms, the proportion of immobile protons p and $\int_0^{2\pi/Q_{max}} P(a)da$ both represent the same atoms that are immobile (at the resolution of the spectrometer). In the case of a Gaussian distribution $(P(a) = (1/\sqrt{2\pi}s) \times e^{-(a-c)^2/2s^2})$, $\int_0^{2\pi/Q_{max}} P(a)da$ is a non-null function of c and s. Therefore, when using a Gaussian distribution in the Eq. 22, there is a strong correlation between p, c, and s that makes the fit of the EISF difficult. Using a lognormal distribution this problem disappears, since $\int_0^{2\pi/Q_{max}} P(a)da \approx 0$.

The obtained EISF have thus been fitted with the expression

$$A\left(Q, \begin{Bmatrix} p \\ c \\ s \end{Bmatrix}\right) = p + (1-p)\int_0^\infty \frac{1}{s\sqrt{2\pi}a} \times e^{-\frac{(\ln(a/c))^2}{2s^2}} \times \left[\frac{3j_1(Qa)}{Qa}\right]^2 da. \quad (25)$$

RESULTS AND DISCUSSION

Quasi-elastic neutron scattering measurements have been performed at three different temperatures: 15°C (native state), 50°C (C-terminal domain unfolded, N-terminal domain intact), and 70°C (both domains unfolded). As mentioned in the Introduction, the high charge of calmodulin at physiological pH prevents aggregation during thermal unfolding even at concentrations as high as ~90 g/L. The structure of protein solutions has already been investigated by small angle

neutron scattering (SANS) (G. Gibrat, Y. Blouquit, C. T. Craescu, and M.-C. Bellissent-Funel, unpublished). In Fig. 1, the SANS spectrum of the 86 g/L solution used for QENS experiment is compared to that of a 5 g/L solution. Both solutions are cooled down to room temperature after heating up to 70°C. The SANS spectra are normalized to protein concentration. We notice that there is no increase of intensity at small Q-values. Thus, there is no aggregation, even at 86 g/L. The normalized intensity at 86 g/L is even lower than that at low concentration, demonstrating that there are strong inter-protein repulsive interactions within the protein solution. The absence of aggregation during thermal unfolding is essential for proper studies.

Debye-Waller factors and mean-square displacements

The evolution of the logarithm of the quasi-elastic intensity as a function of Q^2 for the three temperatures is plotted in Fig. 2. As expected, one gets a linear behavior from which the mean square displacements $\langle u^2 \rangle$ have been deduced. One can notice that the evolution of the mean-square displacement is not linear as a function of temperature (in K) (see Table 2). This means that there is a transition in the dynamic behavior of apo-calmodulin between 15°C and 70°C. This dynamical transition can be naturally correlated to the thermal unfolding described previously, since at 15°C apo-calmodulin is native and at 70°C it is almost completely unfolded. Thus, thermal unfolding of apo-calmodulin is not only a structural transition, but also a dynamical one.

Internal motions: EISF and linewidth of internal motions

To determine the nature of this dynamical transition, one has to examine more precisely the temperature behavior of

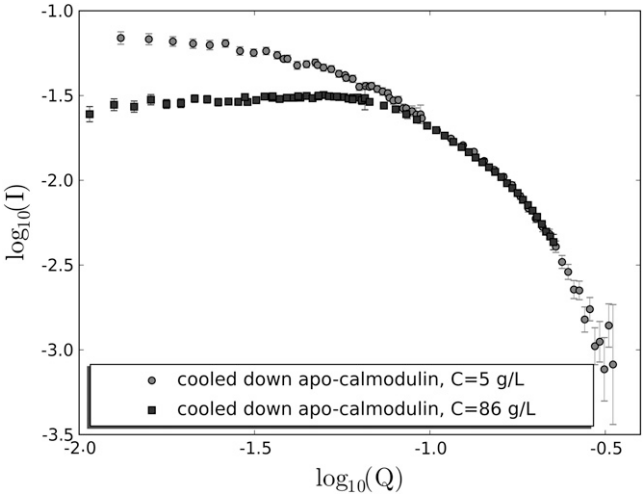

FIGURE 1 $log_{10}(I)$ versus $log_{10}(Q)$ representation of SANS spectra of apo-calmodulin cooled down to room temperature after heating up to 70°C, at 5 g/L (●) and at 86 g/L (○).

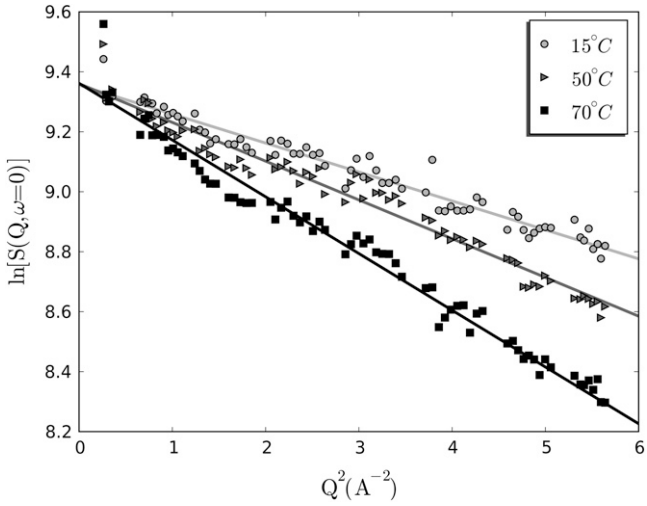

FIGURE 2 Guinier representation of quasi-elastic intensity, $S(Q, \omega = 0)$, or, more precisely, $\int_{|\hbar\omega| \leq 1\ \mathrm{meV}} I_{\mathrm{inc}}(Q, \omega) d\omega$ of apo-calmodulin at several temperatures: ○, 15°C; ▷, 50°C; and □, 70°C. (*Solid lines*) Linear fits leading to the mean-square displacement $\langle u^2 \rangle$. The calmodulin concentration was 86 g/L.

$S_{\mathrm{inc}}(Q, \omega)$. The Fig. 3 shows examples of quasi-elastic spectra fitting, for the two extreme temperatures, 15°C and 70°C, and for two Q-values: 1 $\mathrm{Å}^{-1}$ and 2 $\mathrm{Å}^{-1}$. From the examination of this figure it appears that: Firstly, the EISF, given by the ratio $\mathcal{A}_{\mathrm{L_{diff}}}(Q)/(\mathcal{A}_{\mathrm{L_{diff}}}(Q)+\mathcal{A}_{\mathrm{L_{int}}}(Q))$ (Eq. 17), decreases obviously with Q. Indeed, since the EISF is given by Eq. 20, it must decrease with Q in the adapted Q-range. Secondly, the two Lorentzians, L_{diff} and L_{int}, are wider at high temperature than at low temperature, meaning that motions are faster at high temperature than at low temperature. Finally, the EISF is lower at high temperature than at low temperature, for the two Q values, indicating a decrease of p and/or an increase of $\langle a \rangle$ when increasing temperature.

To be more quantitative, one must examine the parameters given by the fit of $S_{\mathrm{inc}}(Q, \omega)$ using the model of Eq. 8. The obtained values of Γ_{int} and Γ_{diff} at the three temperatures are plotted as a function of Q^2 in Figs. 4 and 5. The experimental EISF is plotted as a function of Q in Fig. 6 and compared with

TABLE 2 Parameters of the model for protein dynamics

T(°C)	15	50	70
T(°K)	288	323	343
$\langle u^2 \rangle$ (Å ^{2})	0.291 ± 0.003	0.387 ± 0.006	0.567 ± 0.006
D_{trans} ($\mathrm{cm}^2\ \mathrm{s}^1$)	(6.5 ± 0.4).10^{-7}	(25.2 ± 1.5).10^{-7}	(44.1 ± 2.0).10^{-7}
$\frac{4\pi}{3}\langle a \rangle^3$ (Å^3)	13.8 ± 0.3	15.1 ± 0.3	16.6 ± 0.3
D_{sph} ($\mathrm{cm}^2\ \mathrm{s}^{-1}$)	(230 ± 20).10^{-7}	(315 ± 30).10^{-7}	(390 ± 30).10^{-7}
p	0.56 ± 0.03	0.25 ± 0.03	0.05 ± 0.03
I_{p}	0.07 ± 0.02	0.84 ± 0.03	2.37 ± 0.04
$\frac{4\pi}{3}\bar{a}^3$ (Å^3)	7.0 ± 0.4	0.9 ± 0.4	0.2 ± 0.4

The mean-square displacement $\langle u^2 \rangle$, the translational diffusion coefficient D_{trans}, the mean volume of spheres $((4\pi)/3)\langle a \rangle^3$, the fraction of immobile protons p, the polydispersity index of spheres volume I_{p}, the most probable volume of sphere $((4\pi)/3)\bar{a}^3$, and the mean diffusion coefficient inside the spheres D_{sph}.

the fits using Eq. 25, at the three temperatures. The inset of Fig. 6 shows the corresponding lognormal distributions. The parameters deduced from the analysis of $S_{inc}(Q, \omega)$ are summed up in Table 2. It appears that the mean volume of spheres in which hydrogen atoms diffuse ($(4\pi/3)\langle a\rangle^3$) and proton diffusion coefficient (D_{sph}) increase, do so with temperature: the mean volume ($(4\pi/3)\langle a\rangle^3$) increases from 13.8 $Å^3$ in the native state up to 16.6 $Å^3$ at high temperature, and the diffusion coefficient (D_{sph}) increases from 230.10^{-7} cm^2/s up to 390.10^{-7} cm^2/s. At the same time, the fraction of immobile protons, p, decreases from 0.56 at low temperature down to almost zero (0.05 ± 0.03) at high temperature. A value of 0.5–0.6 for the fraction of immobile protons is common for native proteins in solution at low temperature (~20°C) (30,31). An almost 0 value for denatured protein in solution had already been found by Russo et al. (11). Another indication of the decrease of the confinement can be found in Fig. 4. Indeed, at 15°C, one gets a flat behavior for Γ_{int} as a function of Q, but at 70°C, Γ_{int} increases at high Q-values. If one refers to Eq. 21, it means that at 70°C, some protons diffuse in spheres with radius $a \gg \pi/Q_{max}$ (Q_{max} is the maximum Q-value of the experiment; 2.4 $Å^{-1}$ in our case). Indeed, atoms diffusing in spheres with radius $a < \pi/Q_{max}$ lead to a flat behavior for Γ_{int} in the Q-range $Q < Q_{max}$. This high-Q increase of Γ_{int} at high temperature is thus coherent with the fact that the radii distribution at high temperature takes non-null values for high radius values. When increasing temperature, and when the protein unfolds, protein protons are less confined than in native state, leading to an increasing number of hydrogen atoms diffusing faster and exploring a larger volume. The remaining fraction of immobile protons of 5% could correspond to some nonlabile protons of the residual secondary structures. At high temperature, most of proton appears mobile, at the resolution of the spectrometer, 180 μeV. Thus, not surprisingly, protons are more mobile in unfolded state than in native state. This mobility increase upon unfolding has already been reported for both backbone (39) and side-chain atoms (40).

The increase of the proportion of mobile protons and of the mean volume of spheres is associated with an increase of the polydispersity of the spheres volumes and a decrease of the volume of the most probable sphere. This can be easily understood if one considers three different populations of protons: the first one is mobile in the native state (protons far from the backbone), the second one appears immobile in the native state but mobile in unfolded states (protons of the backbone and those close to the backbone), and the third one is immobile even in unfolded states (backbone protons belong-

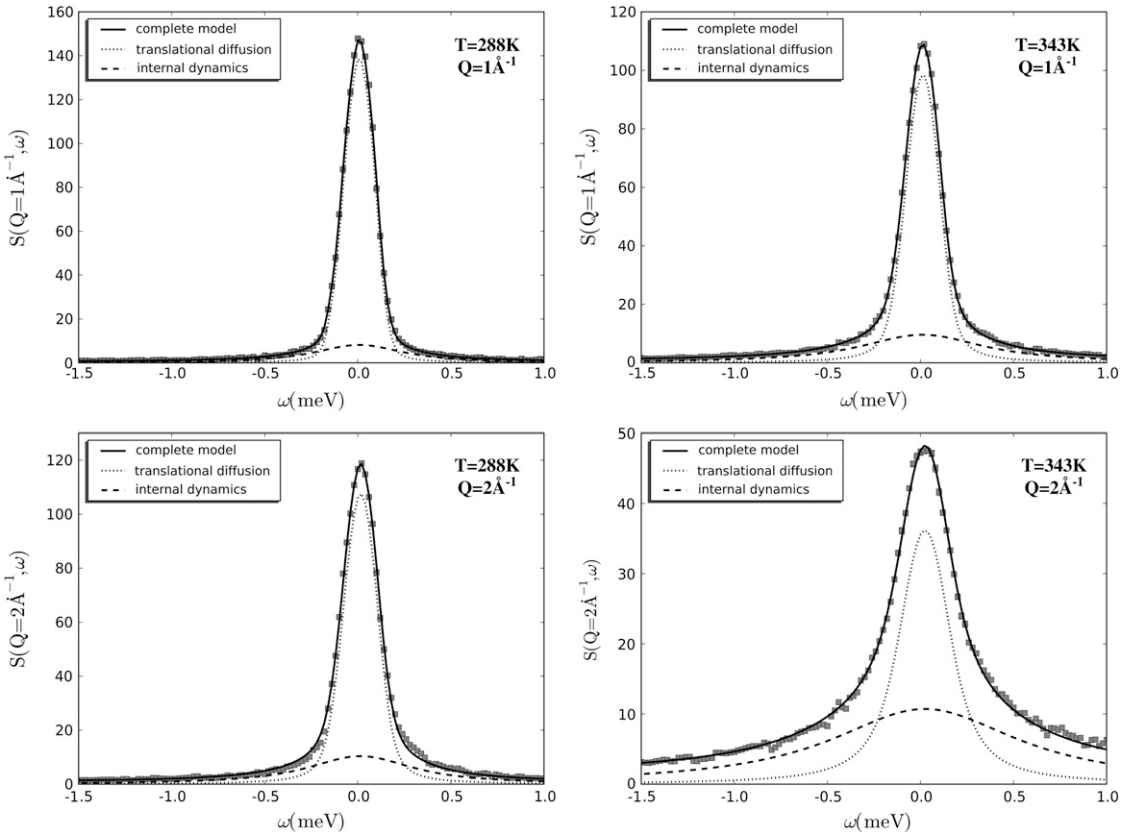

FIGURE 3 Quasi-elastic spectra of apo-calmodulin at two Q-values, 1 $Å^{-1}$ and 2 $Å^{-1}$ and two temperatures, 15°C and 70°C. (*Solid lines*) The fit of the complete model (Eq. 12). (*Dashed lines*) Lorentzian describing internal motions (L_{int}). (*Dotted lines*) Lorentzian describing translational diffusion (L_{diff}). The calmodulin concentration was 86 g/L.

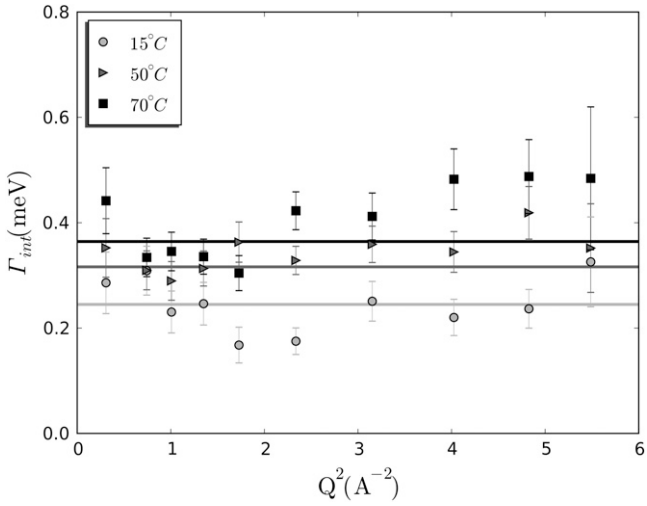

FIGURE 4 Width Γ_{int} of the Lorentzian function describing internal motions, L_{int}, of apo-calmodulin as a function of Q^2 at several temperatures: ○, 15°C; ▷, 50°C; and □, 70°C. (*Solid lines*) Fits in the region $0 < Q < \pi/\langle a \rangle$ leading to the diffusion coefficient D_{sph} (see Eq. 23).

ing to the 10% of secondary structure that still exists at high temperature (41)). The assignment of the three populations is suggested by the results of Carpentier et al. (38). It has been shown that, for an aliphatic chain fixed at one end, the radius of the sphere inside which hydrogen atom diffuses increases linearly with the distance to the fixed end. From NMR experiments, Song et al. (42) also report that atoms of the backbone are less mobile than the atoms of lateral chains. When unfolding apo-calmodulin, we have found a decrease of the proportion of immobile protons, p, a slight increase of the mean volume explored by protons, $((4\pi/3)\langle a \rangle^3$, and a huge increase of the polydispersity index of explored volumes, I_p (from 0.07 at 15°C to 2.37 at 70°C).

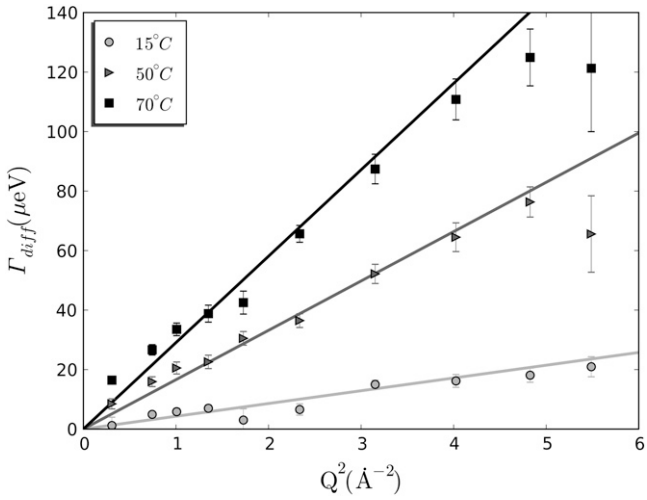

FIGURE 5 Width Γ_{diff} of the Lorentzian function describing global translational diffusion, L_{diff}, of apo-calmodulin as a function of Q^2 at several temperatures: ○, 15°C; ▷, 50°C; and □, 70°C. (*Solid lines*) Linear fits leading to the diffusion coefficient D_t. The resolution of the experiment was 90 μeV (HWHM).

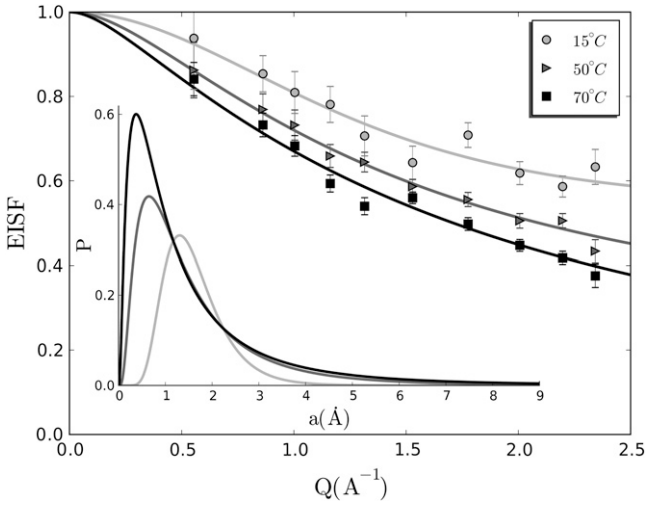

FIGURE 6 Elastic incoherent structure factor (EISF) of apo-calmodulin as a function of Q at several temperatures: ○, 15°C; ▷, 50°C; and □, 70°C. (*Solid lines*) Fits using Eq. 27, leading to the immobile protons proportion p, the mean radius of spheres in which hydrogen atoms diffuse $\langle a \rangle$, and the polydispersity index of spheres volumes, $I_p = (\sqrt{\langle a^2 \rangle - \langle a^2 \rangle}/\langle a \rangle)^3$. The inset shows the lognormal distributions of sphere radii given by the fit of the experimental EISF.

We can give the following interpretation of these results. When the protein unfolds, the two first populations of protons diffuse faster and explore a volume higher than in the native state. The protons of the second population appear now as mobile, but should explore a volume lower than that of the first population, since they are assumed to be closer to the backbone, and thus to the fixed end (making an analogy with the immobilized alkyl chains of Carpentier et al. (38), the α-carbon can be assimilated to the fixed end of lateral chains). The increase with temperature of the polydispersity of explored volumes reflects the occurrence of the second mobile protons population. Indeed, as one considers only one distribution of sphere radii, one cannot distinguish between these two populations at high temperature, and the parameters given in Table 2 are thus an average over these two populations (formally, one fits two distributions with a single one). To explain the decrease of the most probable volume explored, one has to consider that the volume explored by the second population in the unfolded state is lower than the volume explored by the first population in the native state. For more clarity, this mechanism is schematized in Fig. 7. These considerations are able to explain why there is a decrease of the population of immobile protons and a slight increase of the explored mean volume, as well as the decrease of the most probable volume explored and the huge increase of polydispersity index of the volumes explored.

The strong increase of the polydispersity of the volume of spheres in which atoms diffuse upon unfolding suggests that the dynamics of protein atoms is more influenced by their distance to the backbone than by their solvent exposure. Indeed, if the exposure of solvent to the residue determined

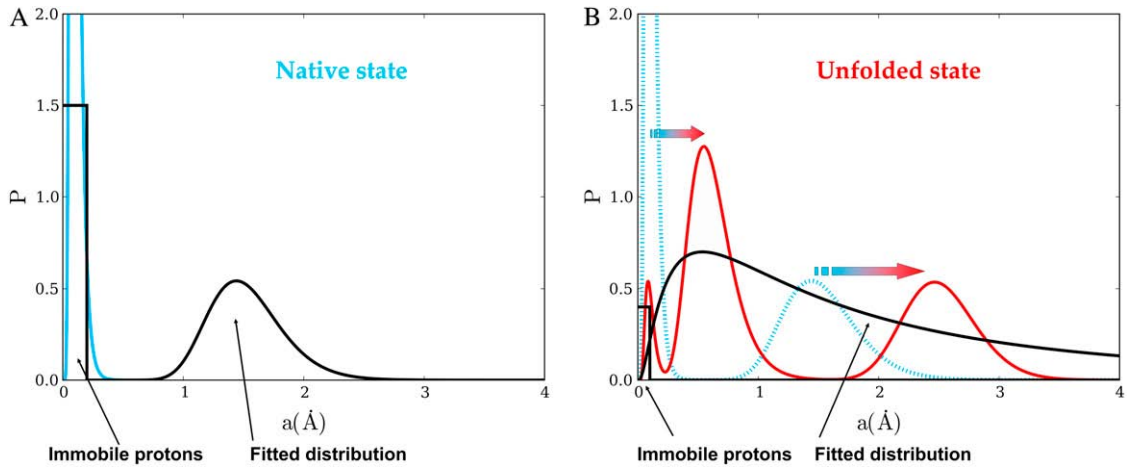

FIGURE 7 Schematic representation of the assumed behavior of the protons populations. (*A*) Native state. (*Blue*) Radii of sphere of the different populations. (*Black*) Fitted model, including a proportion *p* of immobile protons, and a lognormal distribution of sphere radii. (*B*) Unfolded state. (*Red*) Radii of sphere of the different populations. (*Dashed blue line*) Radii of sphere of the different populations in native state. (*Black*) Fitted model, including a proportion *p* of immobile protons, and a log-normal distribution of sphere radii.

dynamics, the dynamics of the unfolded state should be more homogeneous than that of the native state, since in unfolded state, there is no surface and interior: all residues get exposed to solvent. It does not mean that the solvent exposure to the residue does not influence the dynamics. It means that even if both solvent exposure and distance from the backbone influence the dynamics, the distance from the backbone plays a more important role. This is in agreement with the work of Dellerue et al. on native C-phycocyanin protein (36). By combining molecular dynamics simulation and quasi-elastic neutron scattering, the authors account for huge differences in dynamics between backbone and side-chain atoms. They also report smaller differences in dynamics as a function of distance to the center of mass of the protein, i.e., between protein surface and interior. Differences in dynamical behavior of backbone atoms and side-chain atoms have also been reported by Song et al. (42), using NMR:

> ''Overall, these results are indicative of a view where the polypeptide chain acts as a relatively rigid and highly constrained scaffold while the attached (methyl-bearing) side chains are less restrained, more liquidlike, and moving across smaller barriers.''

As a result of our experiment, to correctly describe protein dynamics, one has to consider at least three populations of protons (and surely more). Due to the experimental uncertainties and to the limited number of Q-values, such fits with several radii distribution would be meaningless.

The distribution of sphere radii

Table 3 gives the number of nonlabile protons of each rank, for each amino-acid type, and for the whole calmodulin. A proton bound to backbone is counted as a zero-rank proton. A proton linked to the first carbon of the lateral chain, just after the carbon α is counted as first rank proton. A proton linked to the second carbon is counted as second-rank proton, etc. For apo-calmodulin, zero-rank and first-rank protons represent 51% of all protons. According to Carpentier et al., these protons must explore lower volumes than higher rank protons. They must also correspond to the 56% of immobile protons in the native state. Mobile protons must be higher rank protons (second-, third-, and fourth-rank protons). Lognormal distribution results when the variable (described by the distribution) is the product of a large number of independent factors. The use of a lognormal distribution is therefore not completely justified. However, the motions of protons of second-, third-, and fourth-rank protons are not independent, and the use of a Gaussian distribution would be even less justified.

Global motions

Native apo-calmodulin has a hydrodynamic radius of 2.5 nm (43). According to the Stokes-Einstein relation ($D_t = kT/6\pi\eta R_h$), one gets a diffusion coefficient of $5.9.10^{-7}$ cm^2/s at 15°C (viscosity of heavy water at 15°C: $\eta_{D_2O} = 1.44$ cP) that is in good agreement with the value of $(6.5 \pm 0.4).10^{-7}$ cm^2/s reported in this work (from Fig. 5 and see Table 2). At high temperature, one has found a radius of gyration of 3.2 nm. If we assimilate unfolded apo-calmodulin to Gaussian chain, that leads to a hydrodynamic radius of 2.6 nm ($R_g/R_h = 1.241$ (44)), and thus to a diffusion coefficient of $\sim 20.10^{-7}$ cm^2/s at 70°C. Here we found a value of $(44 \pm 2).10^{-7}$ cm^2/s. The agreement is not as good as that for the native state. But the width of the Lorentzian associated with the diffusion, Γ_{diff} is quite low and at the limit of the resolution, such that the value of diffusion coefficient obtained is not precise. One can also

TABLE 3 Gives the number of nonlabile protons of each rank, for each amino-acid type, and for whole calmodulin

Residue	Rank 0	Rank 1	Rank 2	Rank 3	Rank 4	Occurrence
Ala	2	3	0	0	0	11
Arg	1	2	2	2	0	6
Asn	1	2	0	0	0	6
Asp	1	2	0	0	0	17
Cys	1	2	1	0	0	0
Glu	1	2	2	0	0	6
Gln	1	2	2	0	0	21
Gly	2	0	0	0	0	11
His	1	2	2	0	0	1
Ile	1	1	5	3	0	8
Leu	1	2	1	0	6	9
Lys	1	2	2	2	2	8
Met	1	2	2	0	3	10
Phe	1	2	5	0	0	8
Pro	7	0	0	0	0	2
Ser	1	2	0	0	0	4
Thr	1	1	3	0	0	12
Trp	1	2	5	0	0	0
Tyr	1	2	4	0	0	2
Val	1	2	6	0	0	7
Occurrence	183	263	279	52	100	
Fraction	21%	30%	32%	6%	11%	

A proton bound to backbone is counted as a zero-rank proton. A proton linked to the first carbon, after the carbon α, is counted as the first-rank proton. A proton linked to the second carbon after the carbon α is counted as the second-rank proton, and so forth. Special cases: all protons of prolines are counted as zero rank. All protons of aromatic cycles are counted as belonging to the same rank: i.e., that of the first carbon of the cycle. Nitrogen and sulfur atoms are taken into account in the same way as the carbon atoms for establishment of ranks. All OH, NH, and NH_2 hydrogens are assumed to be labile.

notice that, in the unfolded state, the width Γ_{diff} is not perfectly linear with Q^2. This pleads in favor of another assumption to explain the observed discrepancy at high temperature: the model of Brownian diffusion is less justified in the unfolded state than in the native one. In other terms, the assumption of absence of coupling of translational diffusion and internal motions is well justified for compact proteins, but is less adapted to polymerlike objects, which are highly flexible and do not diffuse like rigid objects. Analogous difficulties in describing unfolded protein internal dynamics, due to the coupling of global and internal motions, are reported by Wirmer et al. (45).

CONCLUSION

The use of QENS has allowed us to exhibit a dynamical transition associated with thermal denaturation of apo-calmodulin. This dynamical transition goes with an increase of the protein picosecond-timescale dynamics, and with a decrease of the confinement of hydrogen atoms. Moreover, it appears that thermal unfolding is associated with an increase of the mean volume explored by atoms, but also with a decrease of the most probable volume explored and a considerable increase of the polydispersity of the picosecond-timescale dynamics of protein atoms. This suggests that the distance of atom to protein backbone plays a more important role than the solvent exposure to the residue, or the fact that the residue belongs to protein surface or interior in determining atom dynamics in proteins. However, this experiment also shows that to properly describe the dynamics of apo-calmodulin, one has to consider several distributions of radii of spheres, and thus several distributions of atomic dynamic behavior corresponding to several classes of atoms. Data with higher statistics and with more Q-values are required to use such models. Moreover, data at higher Q-values would be useful to validate the model used here. Indeed, the major differences between all different possible models, with Gaussian, lognormal, or other distributions, and considering atoms diffusing inside spheres or diffusing on spheres, or considering other kind of atom motions, are expected to lie at high Q-values. Finally, in the unfolded state, almost all protons of apo-calmodulin are mobile at a resolution of 180 μeV, whereas, in the native state, only ~45% of them are mobile.

We thank Jean-Marc Zanotti, who helped us in performing QENS experiments on the MIBEMOL spectrometer of Reactor Orphée of Laboratoire Léon Brillouin.

REFERENCES

1. Levinthal, C. 1968. Are there pathways for protein folding. *J. Chim. Phys.* 65:44–45.
2. Privalov, P. L. 1996. Intermediate states in protein folding. *J. Mol. Biol.* 258:707–725.
3. Ptitsyn, O. B. 1995. Structures of folding intermediates. *Curr. Opin. Struct. Biol.* 5:74–78.
4. Karplus, M., and D. L. Weaver. 1994. Protein-folding dynamics—the diffusion-collision model and experimental data. *Protein Sci.* 3:650–668.
5. Dill, K. A. 1999. Polymer principles and protein folding. *Protein Sci.* 8:1166–1180.
6. Schellman, J. A. 2002. Fifty years of solvent denaturation. *Biophys. Chem.* 96:91–101.
7. Yon, J. M. 1997. Protein folding: concepts and perspectives. *Cell. Mol. Life Sci.* 53:557–567.
8. Frauenfelder, H., G. A. Petsko, and D. Tsernoglou. 1979. Temperature dependent x-ray diffraction as a probe of protein structural dynamics. *Nature.* 280:558–563.
9. Karplus, M., and G. A. Petsko. 1990. Molecular dynamics simulations in biology. *Nature.* 347:631–639.
10. Rasmussen, B. F., A. M. Stock, D. Ringe, and G. A. Petsko. 1992. Crystalline ribonuclease A loses function below the dynamical transition at 220 K. *Nature.* 357:423–424.
11. Russo, D., J. Perez, J. M. Zanotti, M. Desmadril, and D. Durand. 2002. Dynamic transition associated with the thermal denaturation of a small β-protein. *Biophys. J.* 83:2792–2800.
12. Tehei, M., D. Madern, C. Pfister, and G. Zaccai. 2001. Fast dynamics of halophilic malate dehydrogenase and BSA measured by neutron scattering under various solvent conditions influencing protein stability. *Proc. Natl. Acad. Sci. USA.* 98:14356–14361.
13. Seaton, B. A., J. F. Head, D. M. Engelman, and F. M. Richards. 1985. Calcium-induced increase in the radius of gyration and maximum dimension of calmodulin measured by small-angle x-ray scattering. *Biochemistry.* 24:6740–6743.
14. LaPorte, D. C., B. M. Wierman, and D. R. Storm. 1980. Calcium-induced exposure of a hydrophobic surface on calmodulin. *Biochemistry.* 19:3814–3819.

15. Biekofsky, R. R., S. R. Martin, J. E. McCormick, L. Masino, S. Fefeu, P. Bayley, and J. Feeney. 2002. Thermal stability of calmodulin and mutants studied by ^{1}H-^{15}N HSQC NMR measurements of selectively labeled [^{15}N]Ile proteins. *Biochemistry.* 41:6850–6859.

16. Means, A. R., and J. R. Dedman. 1980. Calmodulin—an intracellular calcium receptor. *Nature.* 285:73–77.

17. Gnegy, M. E. 1993. Calmodulin in neurotransmitter and hormone action. *Annu. Rev. Pharmacol. Toxicol.* 33:45–70.

18. Walace, R. W., E. A. Talant, and W. Y. Cheung. 1980. Assay, preparation, and properties of calmodulin. *In* Calcium and Cell Function, Vol. 1. Academic Press, New York.

19. Protasevich, I., B. Ranjbar, V. Lobachov, A. Makarov, R. Gilli, C. Briand, D. Lafitte, and J. Haiech. 1997. Conformation and thermal denaturation of apocalmodulin: role of electrostatic mutations. *Biochemistry.* 36:2017–2024.

20. Masino, L., S. R. Martin, and P. M. Bayley. 2000. Ligand binding and thermodynamic stability of a multidomain protein, calmodulin. *Protein Sci.* 9:1519–1529.

21. Reference deleted in proof.

22. Yang, A., S. Miron, P. Duchambon, L. Assairi, Y. Blouquit, and C. Craescu. 2006. The N-terminal domain of human centrin 2 has a closed structure, binds calcium with a very low affinity, and plays a role in the protein self-assembly. *Biochemistry.* 45:880–889.

23. Tjandra, N., H. Kuboniwa, H. Ren, and A. Bax. 1995. Rotational dynamics of calcium-free calmodulin studied by ^{15}N-NMR relaxation measurements. *Eur. J. Biochem.* 230:1014–1024.

24. Zanotti, J. M., G. Herve, and M. C. Bellissent-Funel. 2006. Picosecond dynamics of T and R forms of aspartate transcarbamylase: a neutron scattering study. *Biochim. Biophys. Acta Proteins Proteomics.* 1764: 1527–1535.

25. Richard, D., M. Ferrand, and G. J. Kearley. 1996. LAMP, the Large Array Manipulation Program. http://www.ill.fr/data_treat/lamp/front.html. Institut Laue-Langevin.

26. Rols, S. 2001. Qens_fit, an IDL routine to fit quasielastic lines using a set of Lorentzian and Gaussian functions. http://whisky.ill.fr/Computing/TOFHR-help/QENS_fit.pdf. Institut Laue-Langevin.

27. Bée, M. 1988. Principles and Applications in Solid State Chemistry, Biology and Materials Science. Adam Hilger, Bristol and Philadelphia.

28. Smith, J. C. 1991. Protein dynamics: comparison of simulations with inelastic neutron scattering experiments. *Q. Rev. Biophys.* 24:227–291.

29. Cusack, S., J. Smith, J. Finney, B. Tidor, and M. Karplus. 1988. Inelastic neutron-scattering analysis of picosecond internal protein dynamics—comparison of harmonic theory with experiment. *J. Mol. Biol.* 202:903–908.

30. Perez, J., J. M. Zanotti, and D. Durand. 1999. Evolution of the internal dynamics of two globular proteins from dry powder to solution. *Biophys. J.* 77:454–469.

31. Zanotti, J. M., M. C. Bellissent-Funel, and J. Parello. 1999. Hydration-coupled dynamics in proteins studied by neutron scattering and NMR: the case of the typical EF-hand calcium-binding parvalbumin. *Biophys. J.* 76:2390–2411.

32. Yang, C., and K. Kuczera. 2002. Molecular dynamics simulations of calcium-free calmodulin in solution. *J. Biomol. Struct. Dyn.* 19:801–819.

33. Torok, K., A. N. Lane, S. R. Martin, J. M. Janot, and P. M. Bayley. 1992. Effects of calcium binding on the internal dynamic properties of bovine brain calmodulin, studied by NMR and optical spectroscopy. *Biochemistry.* 31:3452–3462.

34. Volino, F., and A. Dianoux. 1980. Neutron incoherent scattering law for diffusion in a potential of spherical symmetry: general formalism and application to diffusion inside a sphere. *J. Mol. Phys.* 41:271–279.

35. Fitter, J. 2003. Conformational dynamics of a protein in the folded and the unfolded state. *Chem. Phys.* 292:405–411.

36. Dellerue, S., A. J. Petrescu, J. C. Smith, and M. C. Bellissent-Funel. 2001. Radially softening diffusive motions in a globular protein. *Biophys. J.* 81:1666–1676.

37. Cammon, J. A. M., and S. C. Harvey. 1987. Dynamics of Proteins and Nucleic Acids. Cambridge University Press, Cambridge, UK.

38. Carpentier, L., M. Bee, A. M. Giroudgodquin, P. Maldivi, and J. C. Marchon. 1989. Alkyl chain motions in columnar mesophases—a quasielastic neutron scattering study of di-copper tetrapalmitate. *Mol. Phys.* 68:1367–1378.

39. Farrow, N. A., O. W. Zhang, J. D. Formankay, and L. E. Kay. 1995. Comparison of the backbone dynamics of a folded and an unfolded SH3 domain. *Biochemistry.* 34:868–878.

40. Choy, W. Y., D. Shortle, and L. E. Kay. 2003. Side chain dynamics in unfolded protein states: an NMR based H-2 spin relaxation study of Δ131Δ. *J. Am. Chem. Soc.* 125:1748–1758.

41. Kleinjung, J., F. Fraternali, S. R. Martin, and P. M. Bayley. 2003. Thermal unfolding simulations of apo-calmodulin using leap-dynamics. *Proteins.* 50:648–656.

42. Song, X. J., P. F. Flynn, K. A. Sharp, and A. J. Wand. 2007. Temperature dependence of fast dynamics in proteins. *Biophys. J.* 92: L43–L45.

43. Papish, A. L., L. W. Tari, and H. J. Vogel. 2002. Dynamic light scattering study of calmodulin-target peptide complexes. *Biophys. J.* 83:1455–1464.

44. Oono, Y. 1983. Crossover-behavior of transport-properties of dilute polymer solutions: renormalization group approach. III. *J. Chem. Phys.* 79:4629–4642.

45. Wirmer, J., W. Peti, and H. Schwalbe. 2006. Motional properties of unfolded ubiquitin: a model for a random coil protein. *J. Biomol. NMR.* 35:175–186.